Stimulated Emission in ZnO Nanostructures: A Time-Resolved Study

Aleksandra B. Djurišić,*,† Wai Ming Kwok,‡ Yu Hang Leung,† David L. Phillips,‡ and Wai Kin Chan‡

Departments of Physics and Chemistry, The University of Hong Kong, Pokfulam Road, Hong Kong

Received: May 27, 2005; In Final Form: August 15, 2005

Stimulated emission was studied using time-integrated and time-resolved photoluminescence in ZnO comb, tetrapod, and rod nanostructures. All the measurements were performed on ensembles of the nanostructures. The nanostructures were fabricated by vapor deposition (combs, tetrapods) and hydrothermal methods (rods). While stimulated emission was detected in all of the nanostructures, significant differences in the behavior of the stimulated emission, as well as the lasing threshold power, were found for different morphologies. The differences in the time evolution of the lasing spectra were particularly pronounced. The observed differences in the stimulated emission spectra of the three types of nanostructures in both exciton−exciton scattering and electron−hole plasma regimes are discussed.

Introduction

Because of the large band gap (3.3 eV) and large exciton binding energy in ZnO (∼60 meV), UV exciton lasing is expected at room temperature. Consequently, considerable efforts have been devoted to the study of stimulated emission in ZnO.[1−27] While the theoretical background on the optical processes in direct band gap semiconductors, including emission due to exciton−exciton (E−E) scattering and electron hole plasma (EHP), is well-known,[28,29] in recent years there has been increasing interest in the experimental studies of the stimulated emission from nanostructured materials. Lasing was reported for a variety of ZnO morphologies, such as thin films,[1,2,15−19,21] microtubes,[3,25] nanocoral reefs and nanofibers,[4] whiskers,[5] nanowires,[6,13,14,20,22−24] nanorods,[7−9] nanoribbons,[10,11] nanocombs,[12,13] and tetrapod nanostructures.[26,27] Different lasing mechanisms have been reported as well. The lasing reported in some ZnO films,[2] nanorods,[8] and ZnO nanowires[20] was attributed to random lasing. However, the majority of studies have attributed the lasing to stimulated emission from a resonator formed between the two {0001} facets of the nanostructure.[6] It should be noted that lasing in ZnO was also reported for single nanoribbons,[10,11,14] nanowires,[13,14] and tetrapods,[27] as well as tetrapod nanowires with low tetrapod density (less than 10 tetrapods within laser spot).[26] This is inconsistent with a lasing mechanism involving coherent multiple scatterings, i.e., a random lasing process. However, lasing has been reported from nanostructures in which the position of the second facet serving as a mirror is not entirely clear, such as dendritic nanowire arrays,[12] tetrapods,[27] and tetrapod nanowires.[26] The lasing in a large tetrapod (leg diameter 200−800 nm, leg length 10−30 μm) was found to occur in one tetrapod leg,[27] but the exact position of the second interface serving as a mirror was not identified. Most of the studies have been limited to the lasing at different pumping intensities, while time-resolved studies[1,5,14,15,26,27] have been scarce. Furthermore, the time-resolved measurements using a streak camera were demonstrated to have insufficient resolution to adequately characterize fast stimulated emission processes in ZnO films[1] and nanowhiskers.[5] Johnson et al.[14] performed transient photoluminescence spectroscopy of lasing in ZnO nanowires and nanoribbons for different pump fluences, but the evolution of the spectra with time was not analyzed in detail. Takeda et al.[15] performed the time-resolved photoluminescence measurements of lasing from ZnO thin films, but their analysis was mainly confined to the discussion of the electron−hole plasma emission. Sarko et al.[27] used a novel ultrafast pump−probe technique to characterize lasing in ZnO tetrapods, but in this work a detailed analysis of the time evolution of the emission spectra was lacking.

Thus, different lasing mechanisms, lasing wavelengths and lasing thresholds were reported for all the various ZnO structures, while detailed studies of the ultrafast carrier dynamics have been scarce. The variation in the lasing threshold is expected even for individual nanostructures with the same morphology, due to differences in their dimensions and other properties.[13] Thus, variations in the behavior of nanostructures with different morphologies is expected to be even more pronounced. In this work, we study the stimulated emission in different ZnO nanostructures. ZnO nanocombs, tetrapod nanowires, and nanorods were studied by a time-resolved photoluminescence (TRPL) and time-integrated photoluminescence (TIPL). Two of the morphologies studied (combs and tetrapods) do not show a well-defined cavity bound by two parallel crystal facets. In addition, the nanostructures exhibit different defect related luminescence, green for ribbon/combs and tetrapod nanowires and yellow for nanorods. Thus, a comparative study of the lasing properties in the structures with different morphologies (i.e., different resonator geometry) and different defect levels can help to clarify the factors affecting the stimulated emission in ZnO nanostructures. It should be noted that all the measurements were performed on ensembles of the nanostructures. The estimated number of the nanostructures within excitation area is less than 10 for tetrapod nanowires, around 20−30 for ribbons, and on the order of 1000 for nanorods. The fact that the measurements are made from an ensemble instead of individual nanostructures complicates the analysis of the data, since it is not possible to assign the modes observed to the individual

* E-mail:dalek@hkusua.hku.hk. Fax: +852 2559 9152. Telephone: +852 2859 7946.

† Department of Physics, The University of Hong Kong.

‡ Department of Chemistry, The University of Hong Kong.

10.1021/jp0528055 CCC: $30.25
Published on Web 09/21/2005

cavities. While useful information about the time evolution of the lasing in different nanostructures studied can be obtained, further studies on the individual nanostructures are needed to fully understand the lasing from these structures.

Experimental Section

The ZnO nanorods,[30] tetrapod nanowires,[31] and nanoribbon/comb structures,[32] were prepared as described previously. The ZnO nanorods were prepared by a hydrothermal method from aqueous solution of zinc nitrate hydrate and hexamethylenetetramine. Details of the preparation method are given elsewhere.[30] The tetrapod nanowires were prepared by evaporation of Zn in N_2 gas flow, as described in detail in Ref.[31] The ZnO nanoribbon/combs were prepared by evaporation of ZnO and single wall carbon nanotube mixtures, using a previously reported fabrication method.[32] The morphology of the samples was examined by scanning electron microscopy (SEM) using Leo 1530 field emission SEM.

CW photoluminescence over a wide spectral range was excited by a He−Cd laser (325 nm). Time-resolved photoluminescence (TRPL) was measured by using the Kerr gate fluorescence technique.[33] The experimental apparatus and data analysis methods have been described in detail elsewhere,[33] so only a very brief description will be given here. For the TRPL and TIPL measurements, the samples were excited by a 320 nm laser pulse focused to a spot size of 100 μm diameter. The 320 nm light was generated by mixing of the 800 nm pulse (also used as a gating pulse) and the 532 nm output from a home-built OPA system pumped by the 400 nm second harmonic generation (SHG) of the fundamental laser pulse. Fundamental laser pulses (800 nm) and 400 nm SHG pulse were obtained from a commercial Ti:sapphire regenerative amplifier laser system with a 150 fs pulse duration and a 1 kHz repetition rate. The Kerr gate consisted of a 2 mm cell containing benzene as the Kerr medium which was sandwiched by two crossed polarizers. The instrument response function of this system was about 1 ps. Time-integrated photoluminescence (TIPL) was measured with the same arrangement as the TRPL, except that the gating pulse was blocked and the polarizers were set parallel to each other.

Results and Discussion

ZnO nanorods,[30] tetrapod nanowires,[31] and nanoribbons[32] were prepared according to previously reported procedures. Figure 1 shows the representative SEM images of the three different morphologies studied. It can be observed that tetrapod nanowires consist of a tetrapod with leg diameter in the range 100−200 nm, which decreases with the distance from the core and tapers off into a nanowire with a constant diameter of 20−40 nm. The lengths of the tetrapod core legs are about 1−2 μm, while the wires extend 1−2 μm further. The ribbon/comb structures represent the largest morphology studied here. The ribbons are usually very thin (<50 nm), and combs are somewhat thicker (50−200 nm). The width of the ribbon/combs is usually 1−3 μm, and the length can be in the range 10−20 μm. On the other hand, the ZnO nanorods are the smallest, with the length in the 200−300 nm range, and diameters in the 40−70 nm range. Also, the nanorods exhibit the smallest dispersion of sizes among the structures studied.

All the nanostructures were characterized by TRPL with subpicosecond resolution using a technique described in detail elsewhere.[33] The stimulated emission spectra obtained for the ZnO tetrapod nanowires in the 0−10 ps time range are shown

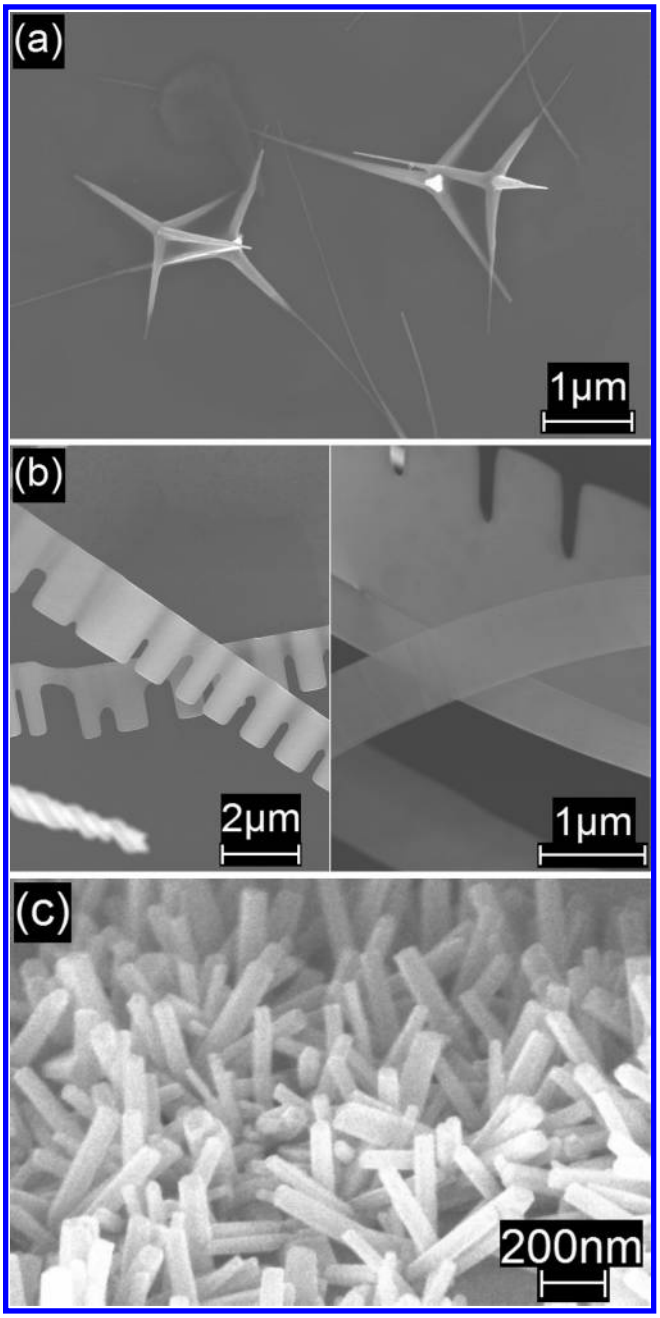

Figure 1. SEM images of ZnO nanostructures: (a) tetrapod nanowires; (b) nanoribbons/nanocombs; (c) nanorods.

in Figure 2. The lasing threshold of these structures is ∼102 μJ/cm^2. The lasing threshold of the tetrapod nanowires is higher than that reported for large tetrapods.[27] The threshold gain can be expressed as[10]

$$g_{th} = \alpha + \frac{1}{2L}\ln^{-1}(R_1R_2) \qquad (1)$$

where L is the length, α is the absorption loss, and R_1 and R_2 are the mirror reflectivities, expected to be ∼0.19 for the ZnO−air interface. Therefore, the shorter structures will obviously require a larger threshold value. Since our tetrapod nanowires have a significantly shorter leg length than that of large tetrapods,[27] a higher lasing threshold is expected. It should also be noted that some differences in the threshold may arise due to different absorption cross sections for different excitation wavelengths (320 nm in our work, and 267 nm in ref 27). Several lasing modes can be observed, and they show rather

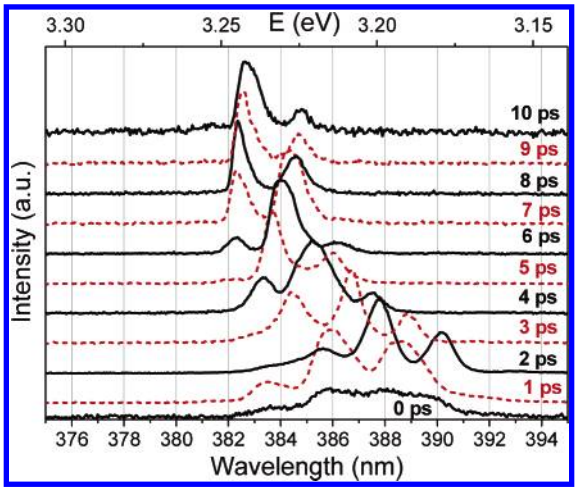

Figure 2. Time-resolved photoluminescence from ZnO tetrapod nanowires in the E−E regime.

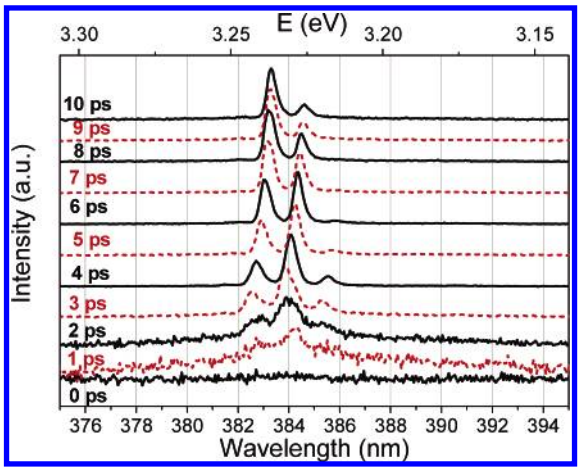

Figure 3. Time-resolved photoluminescence from ZnO nanocombs in the E−E regime.

complex behavior as a function of time. The lasing modes are not equally spaced, which is likely because they represent lasing from different tetrapod nanowires instead of multiple modes from a single tetrapod nanowire. It can also be observed that the lasing modes have larger widths at the beginning of the emission, and they become narrower with increasing time. The line width decreases from 1 to 1.4 nm to 0.5−0.7 nm as the time increases from 1 to 10 ps. This behavior is in agreement with theoretical predictions.[34] It was shown that, unlike semiclassical Markov model, taking into account the coherence of the external light field results in time-dependent line width, so that the spectrum becomes more narrow with increasing time after the laser pulse.[34] Also, the lasing modes appear to shift during the first ∼6 ps, after which the shift becomes negligible.

In the case of the nanoribbon/nanocomb structures, different behavior can be observed, as shown in Figure 3. The lasing threshold in this case is ∼42 μJ/cm^2. The previously reported lasing threshold in ZnO nanoribbon varied in the range 2−25 μJ/cm^2, depending on the ribbon length.[10] We can again observe the narrowing of the lasing modes, but in this case for 5 ps after excitation the initial line width has already been reduced from 0.7 to 0.9 nm to ∼0.4 nm. The shift of the lasing modes still exists, but it is significantly smaller compared to the tetrapods (∼0.5 nm redshift from 2 to 10 ps). Obviously, the ribbon/comb structures are more promising for lasing applications due to their smaller threshold and more narrow lasing modes.

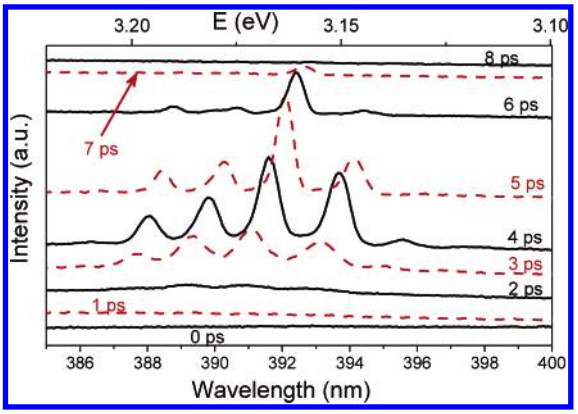

Figure 4. Time-resolved photoluminescence from ZnO nanorods in the E−E regime.

Figure 4 shows the time-resolved spectra of lasing from ZnO nanorods. The lasing threshold was significantly higher, ∼480 μJ/cm^2, which could be expected from the very short rod length. Lasing in ZnO nanorods grown from aqueous solutions was previously reported.[7,9] Govender et al.[7] reported threshold of ∼2.4 mJ/cm^2, but the reported spectra exhibited peculiar features, i.e., the sharp peaks were not confined to the near band-edge region. Choy et al.[9] reported a threshold of ∼140 μJ/cm^2, which is slightly lower than the one reported in our work. This can most likely be attributed to the larger rod size in their work, in agreement with eq 1. From Figure 4 it can be observed that, similar to the previous two cases, the lasing modes at the onset of lasing have larger line width (0.9−1 nm), and they become more narrow (∼0.6 nm at 5 ps). Unlike the previous two cases, the lasing modes have similar delay and decay times. This can be attributed to a smaller variation in the rod sizes compared to the tetrapods and ribbon/combs. It was reported for ZnO nanoribbons that the majority of the ribbons with a length smaller than 6 μm could not support lasing.[10] It was also reported that no clear lasing was observed in nanowires with diameters under 130 nm and lengths smaller than 2 μm.[13] Therefore, the lasing from the nanorods with such small dimensions as obtained here and reported by Choy et al.[9] requires rather a large gain, approaching 10^4 cm^{-1}.[13] If we disregard the absorption losses in eq 1 and assume a rod length of 300 nm, we can obtain an estimated threshold gain of ∼0.5 × 10^4 cm^{-1}. The variation of the threshold for the nanostructures with different morphologies studied here is in reasonable agreement with the expected 1/L dependence. However, it is still possible that some nanostructures either with exceptionally good crystal quality or with poor crystal quality would deviate from expected behavior based on their size.

With an increasing excitation power, all three morphologies exhibit broadening and a significant increase in the emission intensity, which would be expected for a transition from lasing in the E−E scattering regime to lasing in the EHP regime. The time-resolved spectra obtained for the tetrapod nanowires are shown in Figure 5. We can see that the broad, intense emission shows some red shift in the first 3 ps, and then at longer times slightly shifts to the blue. This is in agreement with the reported behavior of EHP lasing in ZnO thin films.[15] If we compare the emission spectra in the E−E and EHP regimes at later times (for example 10 ps) we can observe that the emission in the EHP regime is red-shifted compared to the E−E lasing modes, in agreement with other reports in the literature.[1,9,13,15,16,27] The red-shift of the EHP emission is typically attributed to the band gap reduction due to Coloumb interactions among the free carriers.[9,27] The blue shift at later times can be attributed to the

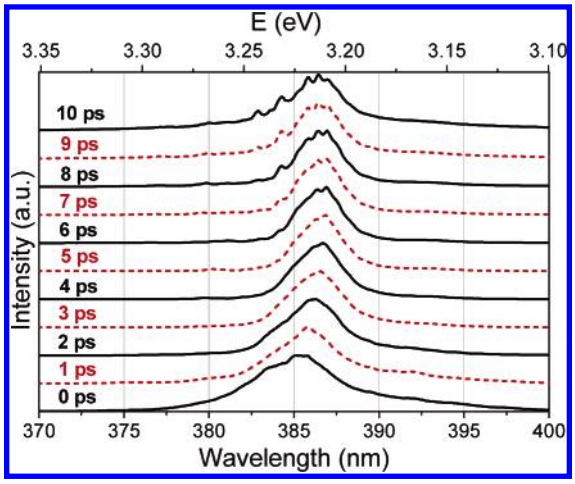

Figure 5. Time-resolved photoluminescence from ZnO tetrapod nanowires in the EHP regime.

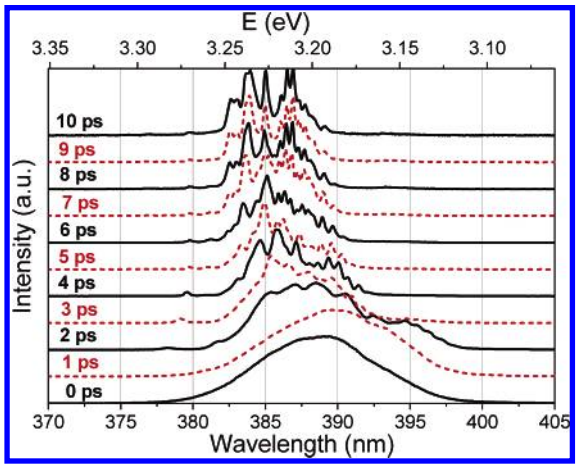

Figure 6. Time-resolved photoluminescence from ZnO nanocombs in the EHP regime.

band gap recovery due to a decreasing carrier density.[15] Also, at later times, some structure in the broad EHP peak can be observed. The threshold for the EHP emission was ~315 μJ/cm^2.

Figure 6 shows the TRPL spectra of the ribbon/comb nanostructures in the EHP regime. The threshold was ~126 μJ/cm^2. Similar behavior to that of the tetrapod nanowires can be observed, except that the emission spectrum shifts faster. The peaks first shift to the red at 1 ps, and then start shifting back to the blue from 2 ps. At 10 ps, a structured emission can be observed at similar positions to the E−E emission. Coexistence of stimulated emission in the E−E and EHP regimes was previously reported in ZnO thin films,[1] and it was attributed to the spatial nonuniformity of the sample. However, our results indicate that the coexistence of the lasing in these two regimes is a result of the faster decay of the EHP emission and the blue-shift of the emission after 1−2 ps due to a decrease in the free carrier concentration and a consequential band gap recovery. The coexistence of the EHP and the exciton−exciton scattering was also previously reported in semiconductor quantum well structures.[35]

Figure 7 shows the emission in the EHP regime from ZnO rods. The threshold pump fluence corresponding to the appearance of the broad and intense emission was 900 μJ/cm^2. It can be observed that in this case there is no significant shift of the emission with time, similar to the behavior of the E−E lasing in rods. However, some structure in the broad peak can be observed already after 2 ps. If we compare the spectra at similar

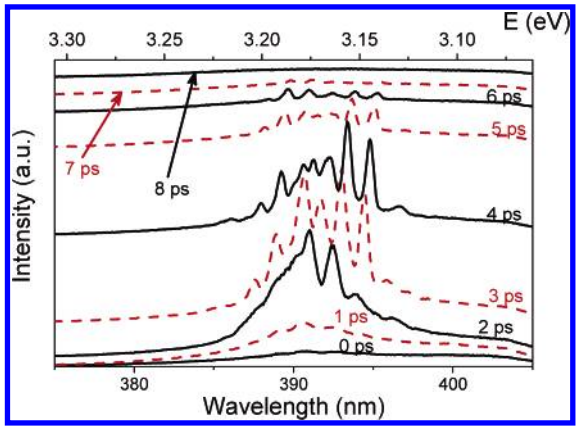

Figure 7. Time-resolved photoluminescence from ZnO nanorods in the EHP regime.

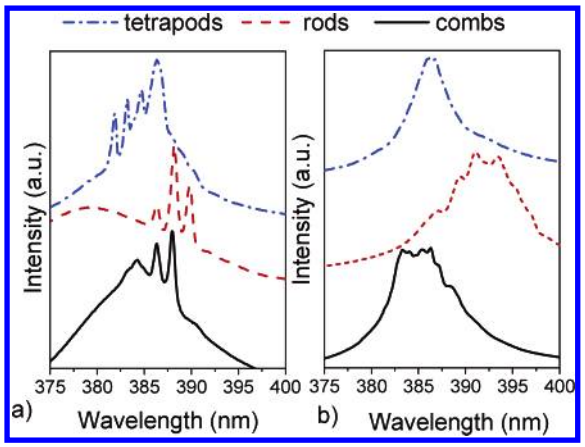

Figure 8. Time-integrated photoluminescence from ZnO nanostructures in (a) the E−E regime and (b) the EHP regime.

time scales (i.e., 4 ps in the E−E regime and the EHP regime), the shift between the peaks is rather small. However, if we compare the peak positions in the integrated spectra, the red shift between the lasing in the E−E and EHP regimes is evident. The TIPL spectra of tetrapods, rods, and combs/ribbons are shown in Figure 8. It can be observed that the structure of the broad peak is less evident in the integrated spectra for the EHP regime, which is due to the reduced intensity of the structured emission at longer times. For lasing in the E−E regime, it can be observed that the lasing modes in the ribbon/combs and rods are located at longer wavelengths compared to the spontaneous emission, as expected for an exciton−exciton scattering mechanism. The peak position for exciton−exciton collision where one of the excitons was scattered to the nth exciton level is given by[36]

$$E_n = E_{ex} - E_{ex}^b(1 - 1/n^2) - 3/2kT \qquad (2)$$

where $n = 2, 3, \ldots$ and $E_{ex}^b = 60$ meV is the exciton binding energy. However, this is not the case for the emission from the tetrapod nanowires. This is possibly due to the variation in the position of E_{ex} for individual tetrapods. Since there is a larger number of tetrapod nanowires contributing to the spontaneous rather than to the stimulated emission, it is not possible to draw reliable conclusions on the relative peak positions in the spectra taken from large number of tetrapod nanowires. It should also be noted that even though the lasing was measured from an ensemble of the nanostructures, the mode widths have been rather narrow (0.4−0.5 nm for ribbon/combs, 0.6 nm for nanorods, and 0.6−0.8 nm for tetrapod nanowires), which is

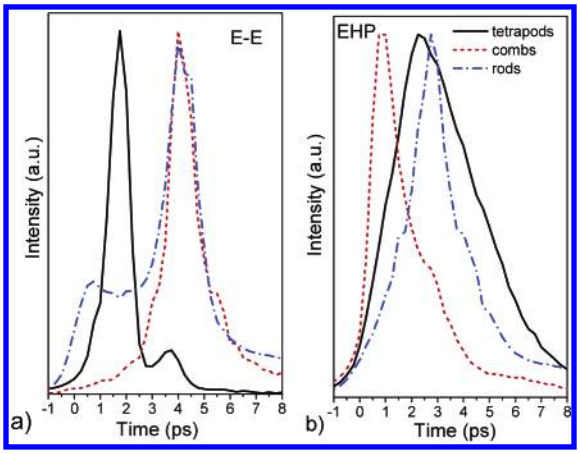

Figure 9. Decay curves for ZnO tetrapod nanowires, combs, and rods in (a) the E−E regime and (b) the EHP regime.

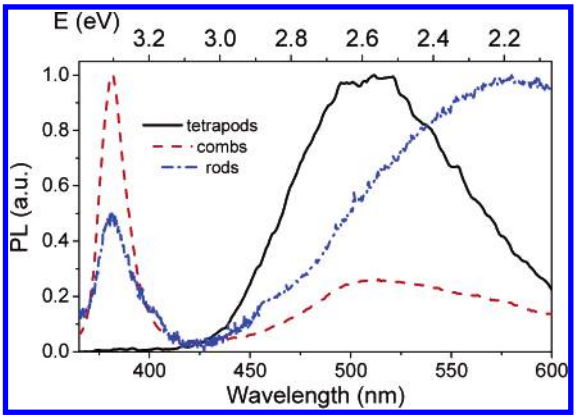

Figure 10. Photoluminescence spectra of the different ZnO nanostructures.

better or comparable to the results reported for ZnO nanowhiskers.[5] Although more narrow emission was reported for individual nanowires and nanoribbons,[5,13] it is expected that the lasing modes from multiple nanostructures would be more broad.

Figure 9 shows the decay times of the emission of different ZnO nanostructures in the E−E and EHP regimes. It can be observed that different nanostructures have different delay, rise, and fall times in both regimes. For tetrapod nanowires, we also observed different decay curves at different wavelengths, which often have more than one peak. Multiple peaks in the decay curve from an ensemble of tetrapod nanowires are most likely due to emission from different tetrapod nanowires with each having somewhat different delay times. The delay times for the tetrapod nanowires in the E−E regime vary from 1 to 10 ps, while the decay time is very fast, <1 ps (within instrument response time). Ribbon/combs and rods show similar delay times of ∼4 ps and decay times of ∼1 ps. For lasing in the EHP mode, the combs have the shortest rise time, while the rods have the longest rise time. The decay times of the nanorods and nanoribbon/combs are similar ∼1−2 ps, while the decay time of tetrapods is slightly longer ∼2−3 ps. The rise time of the EHP emission is similar to that in ZnO thin films, which was attributed to the cooling of hot carriers to a quasi-thermal equilibrium.[15] The longer delay times for emission in the E−E regime are in agreement with the results for nanowires and nanoribbons, where longer delay times were attributed to the longer times needed to achieve a high concentration of excitons in the excited state.[14] Since different individual nanostructures have different delay times,[14] it is difficult to draw conclusions from the decay of lasing in the E−E regime, other than the fact that decay times for all nanostructures are short. For the EHP regime, further studies on individual nanostructures are needed to establish whether there is any significant correlation between the size and the rise time for the EHP emission.

The data obtained indicate that the lasing threshold in the three types of nanostructures studies here is mainly dependent on the nanostructure size. The nanostructures studied here have very different morphology, and also very different defect emission, as shown in Figure 10. All the structures show some defect emission, green for ribbons and tetrapod nanowires and yellow for the rods. The origin of the defect emissions in ZnO is controversial.[37] Several different hypotheses, such as oxygen vacancy, copper impurities, antisite oxygen, etc. for green emission[37] and interstitial oxygen and Li impurities for yellow emission[30] were proposed in the literature. Most likely, two different defects are responsible for the green and yellow emissions, with green emission involving surface defects and yellow emission involving defects in the bulk.[30] Since the ratio of the defect emission to the UV emission decreases as the excitation power increases,[37] the existence of defect emissions does not have a significant effect on the stimulated emission. However, the existence of native defects, such as native shallow donors, is expected to affect the carrier concentration and thus can affect the carrier dynamics. The existence of shallow donors can be investigated by electron spin resonance (ESR) spectroscopy, since shallow donors are expected to produce a peak at $g \sim 1.96$.[30,37] For the ZnO nanorods, a strong peak at $g = 1.96$ was obtained, while no signal was obtained for the tetrapod nanowires, indicating considerably higher shallow donor concentration in nanorods. ESR on nanoribbons could not be performed due to difficulties in the sample preparation, i.e., obtaining a sufficient quantity of free-standing nanoribbons in a powdered form. Since the transition from exciton to EHP dynamics is expected to happen at a carrier density higher than the Mott density (∼4×10^{18} cm^{-3} in bulk ZnO),[14] the differences in the carrier concentrations in different ZnO nanostructures are expected to affect the carrier dynamics. It should also be noted the excitonic effects at carrier concentrations above the Mott density have been reported in quantum wires,[38] which was attributed to the stabilization of excitons in reduced dimensionality. Thus, it is possible that the morphology of the samples will affect the carrier dynamics. At present, it is not possible to distinguish whether the observed differences in the carrier dynamics are a result of different electronic properties or different morphologies of the nanostructures.

Conclusions

We have studied lasing in different ZnO nanostructures using time-integrated and time-resolved photoluminescence. Despite the different morphologies and optical properties of the nanostructures investigated, the lasing threshold was found to be mainly dependent on the average size of the nanostructures. On the other hand, the behavior of the emission spectra over time greatly varied for different nanostructures. Differences in behavior were observed in both the exciton−exciton scattering and electron hole plasma lasing regimes. While some of the differences can be attributed to the variation in morphological properties, there is a complex relationship between the nanostructure properties and ultrafast carrier dynamics. Further studies on single nanostructures are needed to fully explain the differences in time-resolved spectra of the structures with different morphologies.

Acknowledgment. This work is partly supported by the Research Grant Council of the Hong Kong Special Administra-

tive Region, China (Project Nos. HKU 1/01C to D.L.P. and HKU 7019/04P to A.B.D.).

References and Notes

(1) Özgür, Ü.; Teke, A.; Liu, C.; Cho, S.-J.; Morkoç, H.; Everitt, H. O. *Appl. Phys. Lett.* **2004**, *84*, 3223.
(2) Cao, H.; Zhao, Y. G.; Ong, H. C.; Ho, S. T.; Dai, J. Y.; Wu, J. Y.; Chang, R. P. H. *Appl. Phys. Lett.* **1998**, *73*, 3656.
(3) Sun, X. W.; Yu, S. F.; Xu, C. X.; Yuen, C.; Chen, B. J.; Li, S. *Jpn. J. Appl. Phys.* **2003**, *42*, L1229.
(4) Choy, J.-H.; Jang, E.-S.; Won, J.-H.; Chung, J.-H.; Jang, D.-J.; Kim, Y.-W. *Appl. Phys. Lett.* **2004**, *84*, 287.
(5) Qiu, Z.; Wong, K. S.; Wu, M.; Lin, W.; Xu, H. *Appl. Phys. Lett.* **2004**, *84*, 2739.
(6) Huang, M. H.; Mao, S.; Feick, H.; Yan, H.; Wu, Y.; Kind, H.; Weber, E.; Russo, R.; Yang, P. *Science* **2001**, *292*, 1897.
(7) Govender, K.; Boyle, D. S.; O'Brien, P.; Binks, D.; West, D.; Coleman, D. *Adv. Mater.* **2002**, *14*, 1221.
(8) Yu, S. F.; Yuen, C.; Lau, S. P.; Park, W. I.; Yi, G.-C. *Appl. Phys. Lett.* **2004**, *84*, 3241.
(9) Choy, J.-H.; Jang, E.-S.; Won, J.-H.; Chung, J.-H.; Jang, D.-J.; Kim, Y.-W. *Adv. Mater.* **2003**, *15*, 1911.
(10) Yan, H.; Johnson, J.; Law, M.; He, R.; Knutsen, K.; McKinney, J. R.; Pham, J.; Saykally, R.; Yang, P. *Adv. Mater.* **2003**, *15*, 1907.
(11) Bando, K.; Sawabe, T.; Asaka, K.; Matsumoto, Y. *J. Lumin.* **2004**, *108*, 385.
(12) Yan, H.; He, R.; Johnson, J.; Law, M.; Saykally, R. J.; Yang, P. *J. Am. Chem. Soc.* **2003**, *125*, 4728.
(13) Johnson, J. C.; Yan, H.; Yang, P.; Saykally, R. J. *J. Phys. Chem. B* **2003**, *107*, 8816.
(14) Johnson, J. C.; Knutsen, K. P.; Yan, H.; Law, M.; Zhang, Y.; Yang, P.; Saykally, R. J. *Nano Lett.* **2004**, *4*, 197.
(15) Takeda, J.; Kurita, S.; Chen, Y.; Yao, T. *Int. J. Mod. Phys. B* **2001**, *15*, 3669.
(16) Yamamoto, A.; Kido, T.; Goto, T.; Chen, Y.; Yao, T.; Kasuya, A. *J. Cryst. Growth* **2000**, *214*/*215*, 308.
(17) Zhang, X. Q.; Suemune, I.; Kumano, H.; Wang, J.; Huang, S. H. *Appl. Phys. Lett.* **2004**, *96*, 3733.
(18) Liu, X.; Yamilov, A.; Wu, X.; Zheng, J.-G.; Cao, H.; Cheng, R. P. H. *Chem. Mater.* **2004**, *16*, 5414.
(19) Guo, B.; Ye, Z.; Wong, K. S. *J. Cryst. Growth* **2003**, *253*, 252.
(20) Hsu, H.-C.; Wu, C.-Y.; Hsieh, W.-F. *J. Appl. Phys.* **2005**, *97*, 064315.
(21) Segawa, Y.; Ohtomo, A.; Kawasaki, M.; Koinuma, H.; Tang, Z. K.; Yu, P.; Wong, G. K. L. *Phys. Status Solidi B* **1997**, *202*, 669.
(22) Yang, P.; Yan, H.; Mao, S.; Russo, R.; Johnson, J.; Saykally, R.; Morris, N.; Pham, J.; He, R.; Choi, H.-J. *Adv. Funct. Mater.* **2002**, *12*, 323.
(23) Liu, C.; Zapien, J. A.; Yao, Y.; Meng, X.; Lee, C. S.; Fan, S.; Lifshitz, Y.; Lee, S. T. *Adv. Mater.* **2003**, *15*, 838.
(24) Cao, L.; Zou, B.; Li, C.; Zhang, Z.; Xie, S.; Yang, G. *Europhys. Lett.* **2004**, *68*, 740.
(25) Yuen, C.; Yu, S. F.; Sun, X. W.; Xu, C. X.; Leong, E. S. P.; Lau, S. P.; Chen, C. K. *Jpn. J. Appl. Phys.* **2004**, *43*, 5273.
(26) Leung, Y. H.; Kwok, W. M.; Djurišić, A. B.; Phillips, D. L.; Chan, W. K. *Nanotechnology* **2005**, *16*, 579.
(27) Sarko, J. M.; Song, J. K.; Blackledge, C. W.; Swart, I.; Leone, S. R.; Li, S.; Zhao, Y. *Chem. Phys. Lett.* **2005**, *404*, 171.
(28) Klingshirn, C.; Haug, H. *Phys. Rep.* **1981**, *70*, 316.
(29) Hönerlage, B.; Lévy, R.; Grun, J. B.; Klingshirn, C.; Bohnert, K. *Phys. Rep.* **1985**, *124*, 161.
(30) Li, D.; Leung, Y. H.; Djurišić, A. B.; Liu, Z. T.; Xie, M. H.; Shi, S. L.; Xu, S. J.; Chan, W. K. *Appl. Phys. Lett.*. **2004**, *85*, 1601.
(31) Roy, V. A. L.; Djurišić, A. B.; Chan, W. K.; Gao, J.; Lui, H. F.; Surya, C. *Appl. Phys. Lett.* **2003**, *83*, 141.
(32) Leung, Y. H.; Djurišić, A. B.; Gao, J.; Xie, M. H.; Wei, Z. F.; Xu, S. J.; Chan, W. K. *Chem. Phys.* Lett. **2004**, *394*, 452.
(33) Ma, C.; Kwok, W. M.; Chan, W. S.; Zuo, P.; Kan, J. T. W.; Toy, P. H.; Phillips, D. L. *J. Am. Chem. Soc.* **2005**, *127*, 1463.
(34) Kuhn, T.; Rossi, F. *Phys. Rev. B* **1991**, *46*, 7496.
(35) Rubio, J.; Pfeiffer, L.; Szymanska, M. H.; Pinczuk, A.; He, S.; Baranger, H. U.; Littlewood, P. B.; West, K. W.; Dennis, B. S. *Solid State Commun.* **2001**, *120*, 423.
(36) Sun, Y.; Ketterson, J. B.; Wong, G. K. L. *Appl. Phys. Lett.* **2000**, *77*, 2322.
(37) Djurišić, A. B.; Choy, W. C. H.; Roy, V. A. L.; Leung, Y. H.; Kwong, C. Y.; Cheah, K. W.; Gundu Rao, T. K.; Chan, W. K.; Lui, H. F.; Surya, C. *Adv. Funct. Mater.* **2004**, *14*, 856.
(38) Ambigapathy, R.; Bar-Joseph, I.; Oberli, D. Y.; Haacke, S.; Brasil, M. J.; Reinhardt, F.; Kapon, E.; Devaud, B. *Phys. Rev. Lett.* **1997**, *78*, 3579.